# An optical in-situ tool for visualizing and understanding wetting dynamics in membrane distillation

Paul Jacob, Baptiste Dejean, Stéphanie Laborie, Corinne Cabassud

# An optical in-situ tool for visualizing and understanding wetting dynamics in membrane distillation

Paul Jacob[a], Baptiste Dejean [a], Stephanie Laborie[a] and Corinne Cabassud[a]*

[a] TBI, Université de Toulouse, CNRS, INRA, INSA, Toulouse, France

*Corresponding author: corinne.cabassud@insa-toulouse.fr

## Abstract

This paper describes the development of a new optical tool to detect in-situ wetting in membrane distillation. The principle of the detection tool is based on the phenomenon of light transmission. A dedicated experimental setup was developed. The proof of concept of this optical tool is validated using in parallel the Detection of Dissolved Tracer Intrusion (DDTI) method that was previously developed, and which is based on the detection of remaining salt traces in wetted pores by scanning electron microscopy and x-ray dispersion spectroscopy. The in-situ tool was used in standard operating conditions (feed temperature 40°C, laminar flow and vacuum pressure 6 kPa) for vacuum membrane distillation with deionized water, a synthetic saline solution, and seawaters. Controlled wetting was then induced by adding a surfactant in the feed after 30 min of operation and wetting dynamics could be effectively visualized. Additionally, the scalability (macro and mesoscales) of this tool was verified and wetting was visualized at different locations on the membrane surface and compared with the wetting observations made at a global scale. A definition of pore wetting is also proposed.

**Keywords**: wetting; membrane distillation; optical tool; in-situ detection

## Graphical abstract

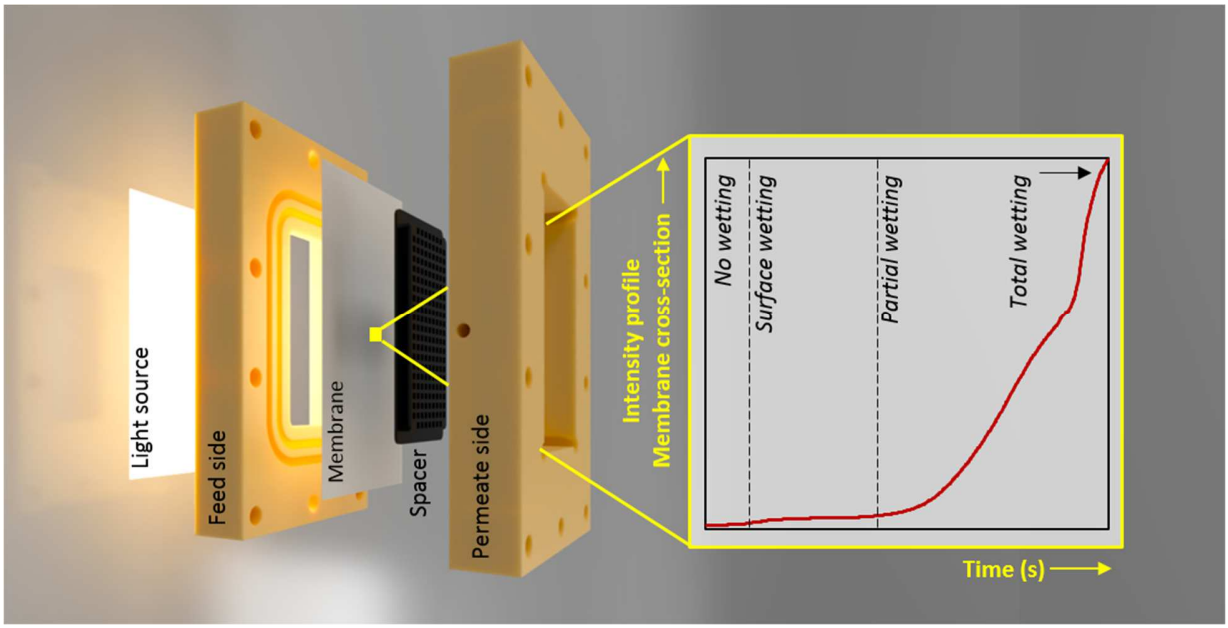


## Highlights

1. In-situ wetting detection tool developed and tested
2. Link between wetting and light transmission established
3. Proportion of liquid intrusion in membrane thickness evaluated
4. Dynamics of pore wetting can be visualized
5. Wetting identified at different scales in-situ

## 1. Introduction

Wetting is an important issue in membrane distillation. Indeed, the risk of wetting occurrence is today one of the major limitations for the industrial development of membrane distillation in various areas, even if the potentiality of MD is very high for process intensification, during the removals of volatile compounds from aqueous mixtures, brines, over-concentration of RO retentates, and better use of energy by coupling with renewable or lost energy sources [1–5]. A recently published literature review focusing on wetting in MD provides all the information about the state of knowledge about wetting mechanisms, causes and effects [6]. It points out that wetting is a crucial challenge in MD and that further assessments are needed.

Membrane distillation exploits the natural or induced hydrophobicity of the polymer used as membranes. As a rule of thumb, porous polymers with low surface energy are selected for MD as they are hydrophobic and ideally do not interact with the feed liquid. However, under adverse conditions, the liquid enters the membrane pores, and the membrane might get "wet".

To be able to make good choices of membranes and operating conditions with the criterion of avoiding wetting, it is indeed necessary to gain knowledge about wetting. To achieve this goal some pertinent tools are required to characterize and to evaluate this phenomenon. It is also very important to define properly and to distinguish the concepts of wettability (risk of wetting occurrence or wetting potential) and wetting (real occurrence of liquid intrusion in pores during MD operation) [7]. Indeed, wetting in membrane distillation is very often understood as the ability of a liquid to maintain contact with a solid surface, resulting from intermolecular interactions when the two are brought together. It is thus more a definition of wettability (or wetting potential) than of wetting itself. Therefore, to better understand and describe this phenomenon in membrane distillation, we have proposed to consider wetting at the pore level and as a localized phenomenon: pore wetting indicates the displacement of the liquid-vapor (L/V) interface inside the membrane pores [7]. Thus, the following definition of pore wetting is considered in this paper:

***"Pore wetting can be defined as the phenomenon where a shift in equilibrium of the liquid/vapor interface promotes liquid intrusion into the hydrophobic pore, i.e., a displacement of the liquid/vapor interface inside the pore, due to the various forces acting upon it, via the interaction of fluid (feed or permeate) and the membrane material under a given operating condition".***

This definition is valid for all membrane distillation configurations.

Today the assessment of wettability is routinely carried out based on such as Liquid Entry Pressure (LEP) and contact angle (CA), according to the terminology definitions that were given by Smolders et al in 1989 [8]. Apart from the fact that these criteria provide information on wettability and not on wetting, these methods are ex-situ measurements from the MD module and require sampling of membranes, that are thus to be destroyed.

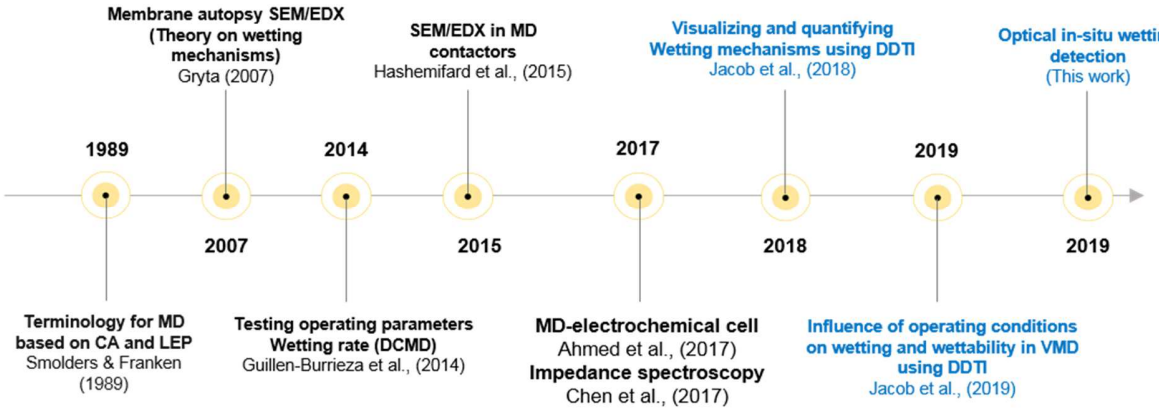


**Figure 1: Literature on wetting and wettability in membrane disitllation and membrane contactors that lead to the current work [6–13]**

In 2007, Gryta developed new approach towards wetting by classifying wetting into various its stage (wetting mechanisms) after observing an autopsy of a wetted membrane by SEM/EDX [9] (Figure 1). Other tools like AFM [14], FTIR [15,16], have also been proposed to characterize wettability and its variation after membrane use, due to fouling or due to membrane aging. All these tools/methods devoted to exploring wettability are *ex-situ*. They can give information on wettability potential on a local scale, however, these tools are unable to give any information on the movement of the liquid-vapor interface leading to wetting. Recently in one of our previous studies, we have proposed a new method called the Detection of Dissolved Tracer Intrusion (DDTI) method [7], that is based on the SEM-EDX detection of traces left by the saline intrusion with the movement of the L/V interface in the membrane pores after the operation. The DDTI method allows to detect wetting mechanisms but it is yet still an *ex-situ* and destructive technique.

On the other hand, significant efforts have been made to develop and adapt non-invasive techniques for classical pressure based membrane processes however they are mainly devoted towards characterizing fouling or scaling [17]. Most of these techniques are not adaptable to membrane distillation for wetting detection. Presently, measuring conductivity [18,19] in the permeate is the most used in-situ wetting detection technique, but wetting can then only be detected when a significant number of pores are completely wetted, which can be too late. Some other technics that are being considered are volumetric methods [20,21], measurement of electric current using a conductive layer on the membrane compartment [11] or impedance across the membrane [12]. All these methods provide only global information. There is an acute need to develop a technique that can combine the advantages of both in-situ and ex-situ techniques and detect localized wetting on the membrane surface during operation.

A comparative assessment of the advantages and disadvantages of the presented methods/techniques for identifying wetting in membrane distillation is presented in **Table 1**.

**Table 1: Comparison between in-situ and ex-situ methods for detecting wetting/wettability**

| Method | Principle | Advantage | Limitation | Information obtained | Ref. |
|---|---|---|---|---|---|
| Contact angle | Surface energy | • Simplicity<br>• Gives immediate information about hydrophobicity of the material and surface tension of sample liquid<br>• Extensively studied | • Higher risk/impact of impurities<br>• Results depend on the consistency of the operator<br>• Not representative only relative to the measured location<br>• Characterizes wettability but not wetting itself | Wettability | [22] |
| LEP | Provoked intrusion of liquid by filtration | • Simplicity<br>• Standardized method<br>• Extensively studied by various authors | • Only gives information on the largest pore<br>• Varies with temperature and feed used | Wettability: Total liquid intrusion | [23]<br>[24] |
| Detection of Dissolved Tracer Intrusion method (DTTI) | Operation with saline solution + detection of saline traces with SEM/EDX | • Local information on wetting<br>• Wetting mechanisms can be identified<br>• User-friendly operation<br>• Fast results<br>• Applicability in several MD configurations | • Ex-situ<br>• Destructive analysis<br>• Preparation of samples can result in artefacts | At local scale, all wetting mechanisms can identified + 2 wetting indicators | [7,13] |
| Conductivity measurement | Conductivity and mass balance | • In-situ<br>• Simple to setup and retrofit into existing pilots<br>• Cheap | • No information on the liquid vapor interface and surface wetting | Wetting: partial / complete wetting at global scale | [18,19]<br>[23]. |
| Volumetric | Mass balance | • In situ<br>• Needs no specialized equipment<br>• Wetting can be studied at operating conditions | • Sensitive<br>• Needs pre-calibrated curve to interpret wetting<br>• Membrane movement inside the cell may affect the reading<br>• Need skilled operator | Wetting: surface / partial wetting at global scale | [21]<br>[20] |

| Method | Principle | Advantage | Limitation | Information obtained | Ref. |
|---|---|---|---|---|---|
| MD - electrochemical cell | Measuring electric current | • In situ<br>• Potential expanded to large scale plants | • Fabricating and maintaining electrically conductive layer<br>• Mass transfer resistance due to the conductive layer | Wetting: partial pore wetting | [11] |
| Electrochemical impedance spectroscopy | Impedance | • In situ<br>• Potential expanded to large scale plants | • Maybe be only useful in DCMD where 2 interfaces are in contact to the membrane surface | Wetting: partial pore wetting and total wetting at global scale | [12] |
| Thermal conductivity detector | Thermal conductivity | • In situ<br>• Used in membrane contactors | • Maybe be only useful in SGMD and VMD applications<br>• Emerging method in membrane contactor; proof of concept for MD still to be developed | Wetting: partial pore wetting | [25–27] |

The objective of this paper is to develop a completely novel approach aiming to visualize wetting in-situ by developing an optical tool based on light transmission. The principle of this method is based on detection of the modification of the refractive index when the L/V interface penetrates inside the membrane pores. The issue is to develop a piece of equipment that can detect this modification and demonstrate that the obtained signal can be related to wetting occurrence. The primary objective of this study is to provide the proof of concept of light transmission to detect localized in-situ wetting in vacuum membrane distillation. Later, we aim to use this tool to study wetting in different feed solutions for a given commercially available membrane and finally an attempt is made to compare and distinguish wetting dynamics at the global scale and to compare it with wetting dynamics at local scale at different locations on the membrane surface under the same operating conditions.

## 2. Principle of light transmission in hydrophobic membrane

For any material, when light falls on it, part of this light is absorbed, transmitted, reflected and scattered. The amount of light scattered versus the amount transmitted determines the transparency of the material. A membrane is a porous matrix of fibers with air inside and surrounding it, implying a membrane with 75 % porosity (ε) is in fact 25 % material (membrane fibers) and the rest is air. Under ambient conditions (standard temperature and pressure, (STP)) when light falls on a sheet of membrane (Refractive index ($N_D$) 1.48 [28]) together with air ($N_D$ 1), the majority of the light rays gets scattered or reflected and only a part of the light gets transmitted through the membrane. This results in a membrane which is opaque white due to light scattering. Light scattering depends on a variety of variables (E.g. intrinsic properties, pore size, uniformity, etc.) including the difference in refractive index between the membrane material and the medium (air) inside/surrounding it. Therefore, if the medium (air) inside the membrane can be replaced by another medium (e.g. water $N_D$ 1.33) with a similar refractive index ($N_D$) as the one of the membrane material, the overall membrane can seem to be translucent and ideally approaching transparent due to this refractive index matching. A described example of this refractive index matching is presented in **Figure 2**. **Figure 2 (a)** visualizes a PVDF membrane, where all the light falling on it is scattered resulting in the membrane to look like an opaque white sheet of plastic similar to a sheet of paper. However, when water was forced into the same PVDF membrane, refractive index matching occurred as the membrane pores were filled with water with a closer refractive index to the membrane one. This results in a membrane translucent with a greater light

transmission (**Figure** 2 (b)). The idea is to exploit this phenomenon in membrane distillation to determine the degree of wetting at a localized scale during operation.

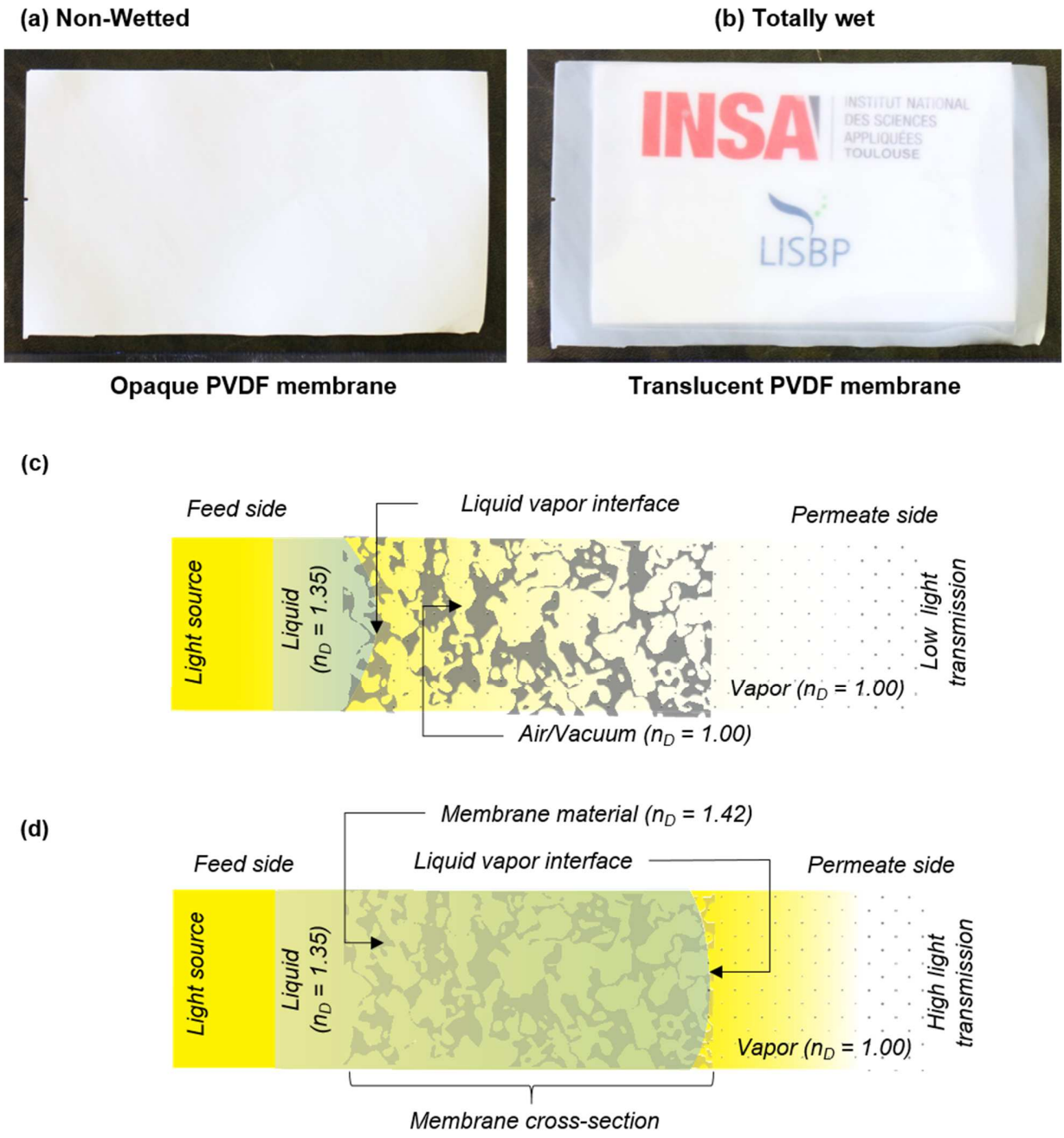


**Figure 2: Light transmission through the same PVDF membrane (a) under non-wetted conditions (b) under totally wetted conditions using water at macro scale. Graphical representation of light**

**tramission through the membrane cross-section at microscale (c) where no wetting had occurred (d) where total wetting has occurred (to be viewed in color)**

To better understand the theory of light transmission in the membrane pores, a graphical representation of a membrane cross-section subjected to vacuum membrane distillation and observed at the microscale is presented in **Figure 2.** The membrane cross-section was illuminated with a light source from the feed side. Here 2 cases are presented. In the case of **Figure 2 (c)**, the liquid-vapor interface is located on the feed side of the membrane. Here the light transmission from the feed side to the permeate side is low due to the miss matching refractive indexes between liquid, membrane and partial air/vacuum inside the membrane cross-section. However, when the interface moves inside the membrane and total wetting occurs on the membrane cross-section (see **Figure 2 (d)**), light transmission increases due to the matching refractive indexes of liquid and membrane material. Thus, light transmission increases, and light scattering reduces significantly. Indeed, the light that was being initially reflected under no wetting condition is now being transmitted by refraction causing the membrane to be ideally transparent while being totally wet. Therefore, by using a camera/or a light sensor, a change in pixel intensity or light intensity can be identified while keeping all the other parameters constant. Exploitation of this phenomenon will result in identifying the movement of the liquid-vapor interface under a steady-state operation of membrane distillation.

## 3. Material and methods

The first step in this study was to design and manufacture an experimental set-up based on both a dedicated module which allowed both to perform VMD with good control of operating conditions and to that allowed light transmission and on optical detection device.

In a second step, it was necessary to define a protocol allowing to detect wetting. For that purpose, it was decided to provoke wetting by adding a surfactant during MD experiments, as surfactants (SDS and Triton X) have been previously reported to induce wetting in membrane distillation [12,29,30]. Our objective is thus to check which is the answer to the optical wetting sensor when the surfactant is injected. It appeared interesting to check at the same time the answer given by wettability indicators and by the DDTI method, for comparison.

### 3.1 The experimental setup: module + optical detection device

The overall MD pilot plant was similar to classical vacuum membrane distillation setup described in our previous paper [7,13]

#### 3.1.1 Special module for light transmission

As presented in **Figure 3 (a)**, the module was designed and fabricated to have viewing windows on both the feed and permeate sides of the membrane module to observe the active membrane surface during operation. The rectangular flat sheet (FS) membrane module was made of two 20 mm C-PVC blocks secured by two 10 mm thick stainless-steel plates. The windows are made in borosilicate glass that could withstand high temperatures with 90 % light transmission for 350 – 2000 nm wavelength.

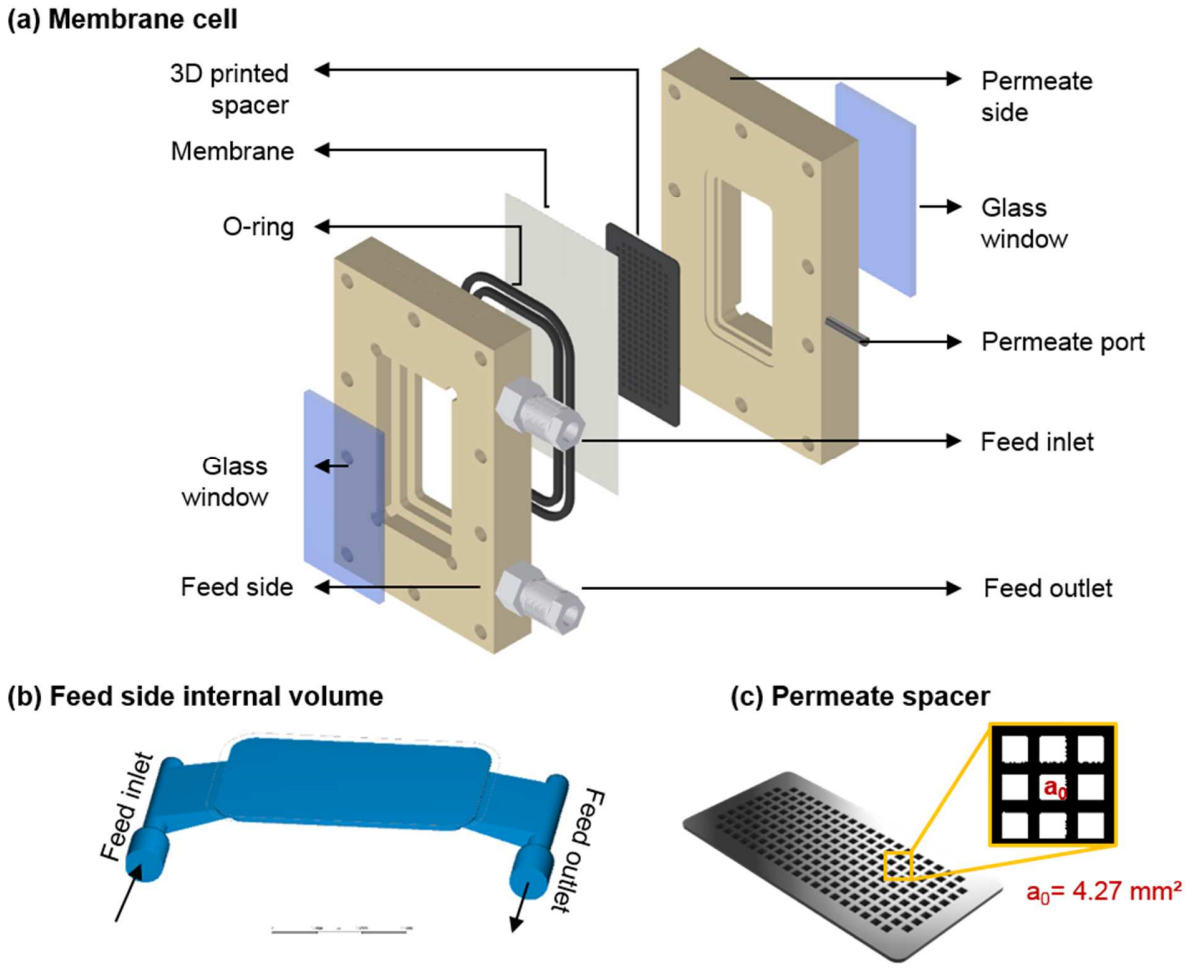

**Figure 3: (a) Special module design (b) feed side internal geometry (c) 3-D printed spacer (to be viewed in color)**

The dimensions of the internal feed side channel were 79 x 41 x 12 mm (length x width x depth) with an edge radius of 7.5 mm. The 3-D printed spacer was only placed on the permeate side of the membrane module to stabilize the membrane during operation. The volume of the internal feed side membrane cell is presented in **Figure** 3 (b). The feed inlet and outlet ports moved to the sides to have the active membrane surface in view and to reduce the impact of hydrostatic pressure at the feed inlet. The enclosed membrane had an active surface area of 3.24 $x10^{-3}$ $m^2$ and was secured by two O-rings on the feed side.

### 3.1.2 Membrane and its characterization

A Durapore membrane ($r_{avg}$ 0.22 µm, PVDF) was used in this study. This membrane has been previously characterized by several authors [31,32]. The virgin membrane was 117.2 ± 0.9 µm thick (δ) with an average porosity 0.75 (ε). The contact angle (CA) and $LEP_w$ of the virgin membrane were 124 ± 2.8° and 2.04 ± 0.86 bar respectively. The Knudsen permeability coefficient ($K_M$) was experimentally determined in this membrane cell using temperature variation method [31] in laminar flow (2.75E-06 ± 1.1E-07 $s.mol^{1/2}.m^{-1}.kg^{-1/2}$) at the reference temperature of 20°C.

### 3.1.3 Design of the membrane support

The advent and accessibility to manufacture custom parts using 3D printing has led to several researchers developing and using custom support designs for membranes processes like RO[33,34] and MD[35]. A 3-D printed support was introduced on the permeate side to support the membrane during operation. The support had 185 openings with an open area ($a_{oi}$) of 4.27 $mm^2$/opening (see **Figure 3 (c)**) determined by image processing. This results in the visualization of only 7.94 $x10^{-4}$ $m^2$ or ~27.4 % of the active membrane surface. All wetting visualizations in this study are limited to these 185 openings or 7.94 $x10^{-4}$ $m^2$ or ~27.4 % of the active membrane surface (A).

### 3.1.4 Optical wetting detection device

The optical system consists of a LED panel, membrane cell, and camera (Basler ace acA1300-200uc with a 16mm lens) (see **Figure 4**). The whole setup was fixed and aligned on an optical rail for stability using optomechanical clamps. The white light LED panel (Metaphase Technologies) was used as the light

source which emitted a uniform intensity. The feed side of the membrane surface faced the light source while the permeate side faced the camera. The camera was focused and calibrated to view the membrane surface through the spacer. Each image was 1200 x 600 pixels in RGB. The overall system has a resolution of 13 pixels/mm or ~77 µm/pixel. The optical setup was designed and manufactured in-house.

During operation, the whole system was placed inside the VMD pilot plant with the feed and permeate ports of the membrane module connected to their respective pumps and setups. The camera recorded images each second for the entire duration of the experiment. The viewing window on the permeate side was heated to avoid vapor condensation on its surface. The whole system was covered with a matte black paper and black fabric to avoid external light interference and signal noise.

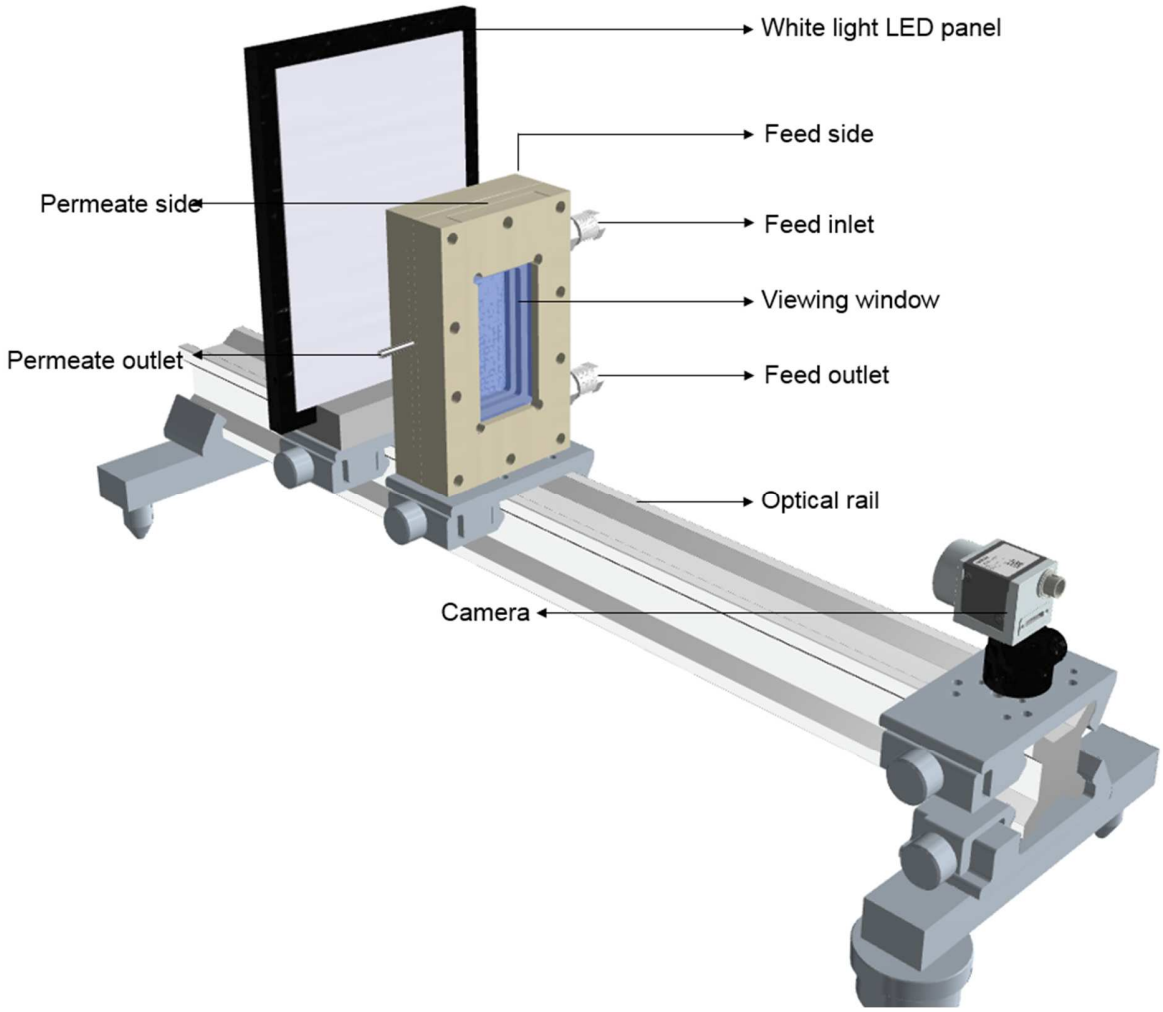

**Figure 4: Optical system for localized wetting visualization (to be viewed in color)**

### 3.2 Protocol of wetting experiments

Each experiment is performed under standardized conditions and is based on 2 successive steps: MD operations are first performed with a given feed solution for the first 30 minutes and then the feed solution is injected with a surfactant under the same operating conditions, with the objective to provoke wetting. The answers of both the MD system (permeate flux, J) and of the optical system are measured on line in the same time.

In this study, laboratory grade Triton X-100 (Sigma Aldrich, France) was used as a wetting inducing agent at 12.5 mg/L for all feed solution samples. The optimal concentration for wetting detection was determined after several tests.

The temperature on the feed side temperature ($T_f$) was fixed at 40±1°C with a feed flow rate (F) ~ Re ≤ 400, while the vacuum pressure was held at 6kPa. The feed solution (cf. 1.1.1) was pre-heated to the desired temperature before circulating on the membrane surface. The vacuum membrane distillation set-up was operated for 1 hour per experiment. For each experiment, the feed solution was circulated in the membrane cell for 30 min. After that, the surfactant was injected into the feed tank to reach a final concentration of 12.5 mg/L. Data for temperature (feed inlet and outlet, permeate), vacuum pressure and conductivities (feed side and permeate flask) were collected and logged during the experimental run. Whereas, images of the membrane surface illuminated from the feed side were taken using a camera on the permeate side at 1 Hz for 1 hour.

#### 1.1.1. 3.2.1 Characterization of feed solution without and with surfactant

4 different feed solutions were studied: de-ionized water (as a control/blank), a synthetic saline solution and two seawaters. The synthetic saline solution was prepared to achieve NaCl concentration ($C_f$) of 35 g/L using crystalline NaCl salt (VWR, France) and deionized water. Seawater were collected at 2 locations in the Mediterranean Sea (Location 42°50'48.0"N 2°56'33.4"E and 43°40'42.1"N 7°13'51.4"E). The samples were analyzed for conductivity, turbidity, pH, UV absorbance at 254 nm. All analytical measurements were performed at least 3 times and the average value is reported in the following table.

**Table 2: Feed solution properties**

| Parameters | Unit | Blank | Synthetic Saline solution | Seawater 1 SW1 | Seawater 2 SW2 |
|---|---|---|---|---|---|
| Conductivity | mS/cm | $5 \times 10^{-5}$ | 51 | 43.8 | 51.1 |
| pH | - | 6.8 | 7.0 | 7.8 | 7.9 |
| Turbidity | NTU | 0.06 | 0.01 | 0.34 | 0.09 |
| UV Absorbance $UV_{254}$ nm | - | 0 | 0 | 0.06 | 0.012 |
| Refractive index | - | 1.33241 | 1.33849 | 1.33754 | 1.33900 |
| Surface tension (ϒ) | mN/m | 72.0 | 73.5 | 73.9 | 72.8 |

Note: All measurements are reported for 25°C

Additionally, surface tension and refractive indexes of the feed solution, and the contact angle of the feed solution on the membrane surface were also analyzed and the protocols are described subsequently (cf. 3.2.2 and 3.2.3). **Table 2** presents the properties of pure water, saline solution and the seawaters termed as SW1 and SW2 respectively. Both seawaters were pre-filtered using a 0.45 µm filter to remove sand and other large particles that may interfere with the measurements. Considering salinity (using conductivity measurements), SW1 was less saline than the synthetic saline solution and SW2.

Here it should also be noted that SW1 was collected from the inlet of a fish farm in a lake adjoining the Mediterranean Sea. This resulted in freshwater or surface water intrusion in SW1 that reduced salinity. It should be noted that SW1 contained higher organics matter as reported by Monnot et. al [36] studying seawater samples from the same location. This is not the case with SW2 where the salinity (measured by conductivity) is similar to the saline solution prepared at 35 g/L NaCl in the lab. Whereas considering pH, water and saline solutions had a pH close to neutral whereas both seawater samples were slightly basic. The surface tension and refractive indexes of all the three solutions were close to the blank solution.

### 3.2.2 Surface tension and contact angle of the feed solutions

The surface tension of the feed solution was measured using the pendant drop method and later the contact angle of these feed solutions with and without surfactants on the membrane surface were also measured using Drop Shape Analyzer – DSA25 (Kruss) at 25°C. The results were post-processed in

accompany software (ADVANCE). Tests were repeated over 10 times with average, and standard deviation reported.

#### 3.2.3 Refractive index

The refractive index ($N_D$) of these solutions were measured at 25°C using a refractometer (RM50 LiquiPhysics, Mettler Toledo). The samples were analyzed over three times with average, and standard deviation reported.

### 3.3 Wettability and wetting indicators

Two classical wettability indicators (Liquid entry pressure ($LEP_w$) and contact angle (CA)) and one wetting indicator from DDTI method previously developed were used in this study. $LEP_w$ and CA characterization were conducted on virgin membranes using feed solutions before and after adding surfactants. Whereas, pore wetting ratio ($\omega_p$), which is defined as the ratio between the depth of liquid intrusion (detected by a tracer) to the total membrane cross-section [7], was used in validating the proof of concept and for interpreting localized wetting visualization into different wetting mechanisms. The acquired images were post-processed in FIJI[37] with the following algorithm (see **Figure 5**).

### 3.4 Treatment of the images obtained from the optical device

From each experiment 3600 images of 1200 x 600 pixel were collected which visualized 27.4 % of the active membrane surface (7.94 $x10^{-4}$ $m^2$) through the spacer and the glass window. The images were taken from the permeate side of the membrane surface with the continuous light source located on the feed side. As an RGB camera is used, the images are converted in 8-bit grayscale.

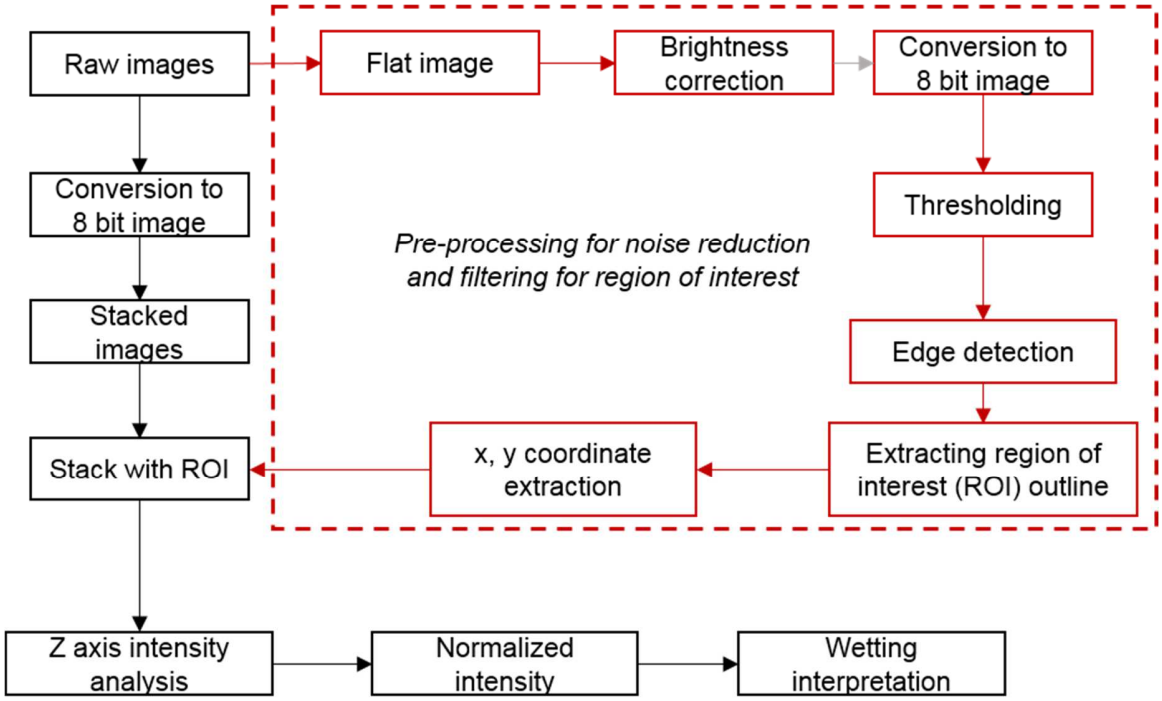


**Figure 5: Flowchart for image processing algorithm for in-situ wetting detection**

A reference image is used to determine the regions of interest (ROI), which correspond to opening surface induced by the membrane support (i.e. the lighted parts in the images). This image corresponds to a steady state operating condition with no wetting. A threshold is applied, followed by a particle analysis [37], which will generate the ROIs from the reference image. The multi measure method from the ROI manager allow the area $S_i$ and the position $(x_i, y_i)$ to be determined for each ROI. Each ROI was labeled from 1-185. An image sequence is then imported corresponding to the experiment on which the ROIs are used in order to determine the mean light intensity $I_{ROI}(x_i, y_i)$ (mean gray value), in each ROI. The intensity was finally normalized for interpreting wetting mechanisms. No further data treatments were conducted as the noise in the acquired data were very low (0.8 – 1.7 gray values).

The averaged intensity values for the ROIs were calculated using *Eq. 3.1* and presented over time.

$$\mathrm{I_{avg}(t)} = \frac{\sum_{i=1}^{M} \mathrm{S_i}.\mathrm{I_{ROI}(x_i, y_i)(t)}}{\sum_{i=1}^{M} \mathrm{S_i}} \qquad \text{Eq. 3.1}$$

Where $I_{avg}$ is the overall average intensity of all region of interests ($I_{ROI}$) observed over time (t). Whereas, $I_{ROI}(x_i, y_i)$ is the average intensity at one ROI at location $x_i$ and $y_i$ with an area $S_i$ observed over time (t). M is the number of ROI's and is here equal to 185.

Additionally, the average intensities were normalized to facilitate the wetting propagation through the membrane cross-section using Eq. 3.2

$$N = \frac{(I_{observed} - I_{initial})}{(I_{max} - I_{intial})} \qquad \text{Eq. 3.2}$$

Where N is the normalized light intensity, $I_{observed}$ is the intensity of one image at time (t) and $I_{max}$ is the intensity of an image captured when total wetting had occurred and finally, $I_{initial}$ was from the reference image where no wetting had occurred after steady-state operation was achieved.

Consider an arbitrary ROI with $S_i$ as the area on the membrane surface with the coordinates $x_i$, $y_i$ at steady state of operation, the liquid vapor interface on the membrane surface and the corresponding light intensity is constant with a low gray value ($I_{initial}$) due to light scattering on the membrane surface. However, when wetting starts to occur the liquid enters the membrane pores in Z axis. As the liquid and the membrane have similar refractive indexes the amount of light transmitted through the membrane is now higher as the relative distance between the light source and the sensor is reduced i.e. at a given $x_i$, $y_i$ coordinate on the membrane surface the camera is picking up a higher light intensity ($I_{observed}$). Finally, when all the liquid has passed through the membrane there is no more increase in light transmission thereby determining the highest intensity value ($I_{max}$). Therefore, by using the above treatment and equations change in light intensity at a known location ($I_{ROI}(x_i, y_i)$) over time maybe used to interpreted into movement of the L/V interface inside the membrane cross-section i.e. Z axis.

### 3.5 Wetting visualization at different scales

Using the above image treatment, we can choose and analyze wetting dynamics (or propagation) at a global or a local scale as presented in **Figure 6**. The evaluations of these scales are detailed in the following paragraphs.

### 3.5.1 Macro scale

If the choice is made to evaluate wetting progression considering all the 185 ROI's as seen in **Figure** 6 (a), wetting analysis using Eq. 3.1 and Eq. 3.2 would be considered at the macro scale or the global scale of the membrane surface. Wetting analysis at this scale would result in an average increase in light intensity of all ROI's in time during the entire duration of the experiment. It should be noted here that the results sections from 4.1 and 4.2 utilizes wetting propagation considering all the ROIs.

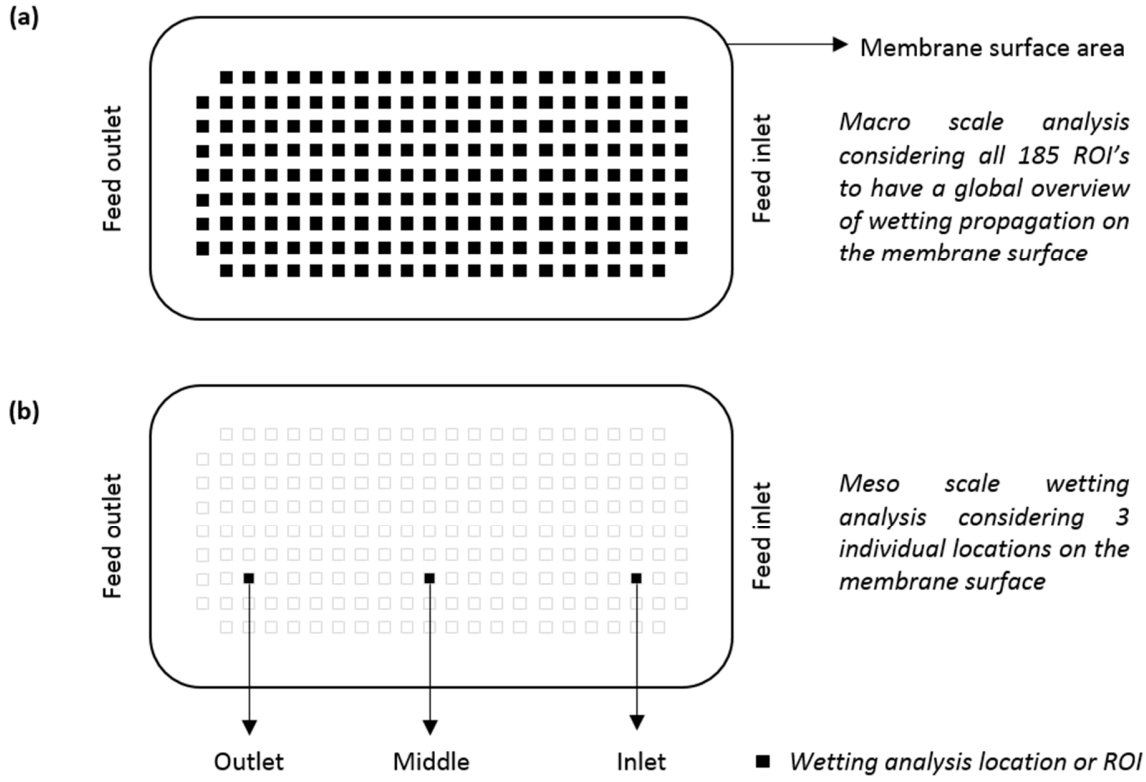


**Figure 6: Wetting analysis with highlighted regions of interest (ROI) (a) at macro scale or global scale (b) at meso scale or local scale**

### 3.5.2 Meso scale

At present, the finest tools that have been developed or used for determining in-situ wetting are at the scale of the membrane. For example, conductivity measurement and recently developed impedance-based technique. The information that can be derived from conductivity measurements is that some pores have been compromised and total wetting has occurred. Wetting is considered at the global scale

of the active membrane surface area and not at a local scale. However, wetting may not occur at all locations simultaneously as it is a localized phenomenon. If such a local analysis is deemed necessary, we can choose to apply the same image treatment algorithm and equations on an individual ROI (4.2 $mm^2$ or at the mesoscale) and have greater detail on wetting at this scale. Therefore, to illustrate the difference in wetting propagation at different scales, 3 ROIs were selected on the membrane surface where; one is close to the membrane surface close to the inlet, one at the middle of the membrane and one close to the outlet of the membrane surface as illustrated in **Figure 6 (b)**. The difference in wetting propagation at these 3 locations will be compared to the wetting propagation at the macro scale to illustrate the effectiveness of this optical tool better.

## 4. Results

### 4.1 Proof of concept of the optical in situ method for wetting detection

The proof of concept of wetting detection using light transmission consisted of provoking wetting on a membrane and observed the drying/de-wetting of the membrane pores using the optical device. These observations can later be validated using pore wetting ratio from the DDTI method previously developed. These observations could then be associated with the wetting mechanisms with the idea to observe the wetting kinetics.

Experiments were conducted by operating the VMD pilot with:

- **Case 1**: A membrane submerged in saline solution ($C_f$ 35 g/L NaCl) with 500 ppm of surfactant for a week to ensure total wetting. Then the membrane was installed inside the membrane module. The change in light intensity was observed through the membrane cross-section during the drying of the membrane for 1 hour. During this time no feed was injected into the membrane cell (as membrane was already wet and would have let water pass through membrane feed side to the permeate side), but a vacuum of 6 kPa was still applied, and all other operating conditions were maintained the same.
- **Case 2**: A reference membrane operated with the synthetic saline solution ($C_f$ 35 g/L NaCl) only, for which no wetting is expected (according to previous results) and observing the change in light intensity for 1 hour through the membrane cross-section during VMD operation.

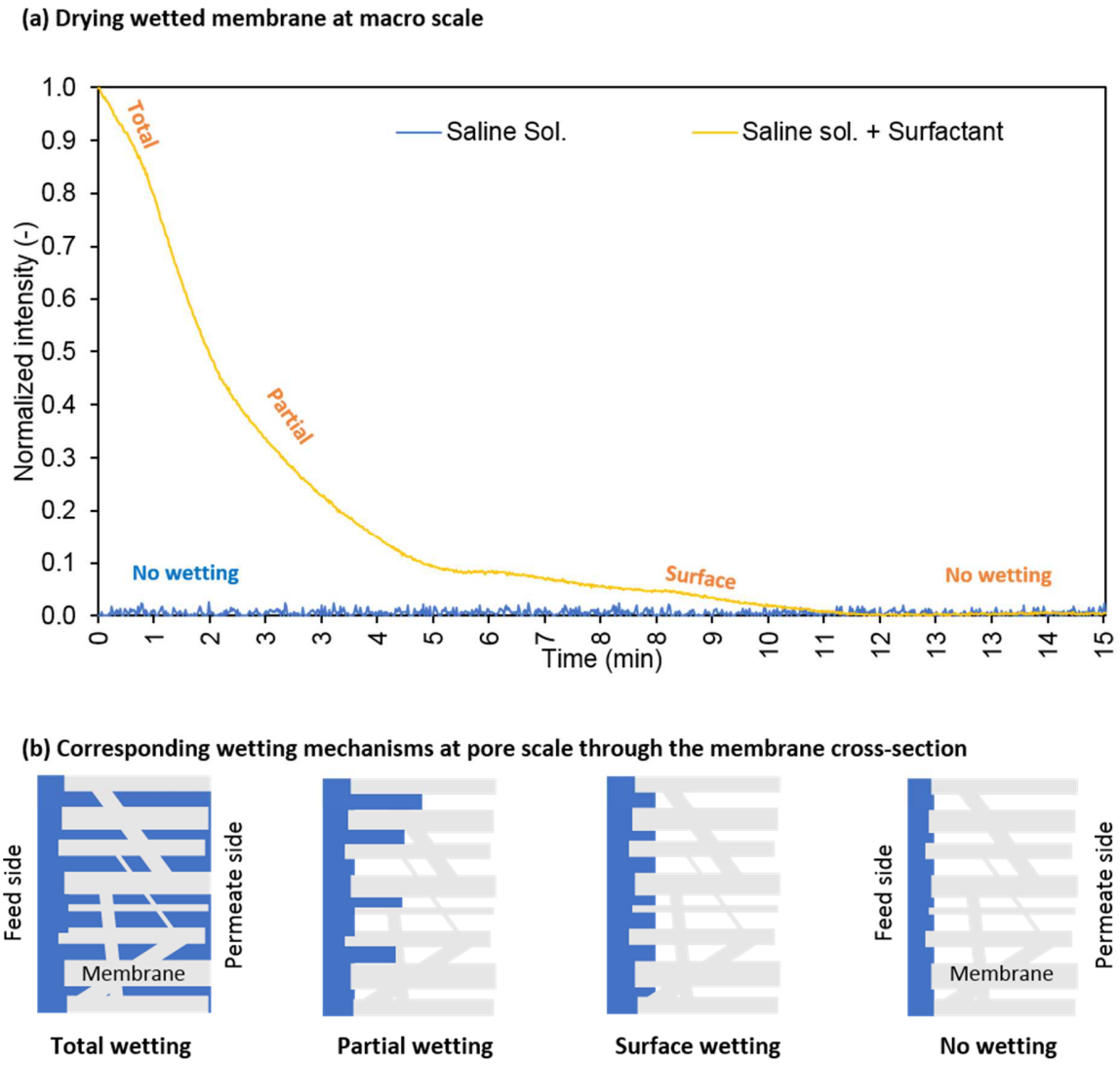


**Figure 7: In-situ visualization and graphical representation of wetting mechanism (to be viewed in color)**

The resulting normalized intensity profiles of these 2 cases are presented in **Figure 7**(a) for 15 min only. Indeed, the membrane subjected to surfactant (case 1) had a higher intensity at the beginning, indicative of total wetting, and as the membrane progressively dried with the water evaporation inside the membrane pores, total wetting probably transitioned to partial wetting, and then to surface wetting . We can suggest that the boundary of transitions between the different wetting mechanisms could correspond to the changes in the curve slope but this assumption needs to be further investigated.

Finally, when all the water had evaporated, and the membrane dried entirely, the intensity reduced to its lowest value indicative of no wetting. At the same time for case 2 where no surfactant was introduced, no wetting was observed during the total experimental duration. These observations are at macroscale but are representative of the transiting wetting mechanisms observed at the pore scale as illustrated in **Figure 7** (b) (for case 1).

To validate the above hypothesis, scanning electron microscopy with X-ray dispersion spectroscopy were conducted on samples acquired from Case 1 and Case 2. Detailed protocols of sample preparation and SEM/EDX analyses can be found elsewhere [7]. An average intensity profiles for Chlorine across the membranes subjected to both cases are presented in **Figure** 8(a) whereas **Figure** 8(b) presents the SEM/EDX micrographs of these membranes. Indeed, high Chlorine traces across the membrane sample subjected to surfactant (case 1) allow validating that total wetting was prevalent in this sample. Whereas for the membrane subjected to the saline solution only (Case 2) no traces of Chlorine on the membrane cross section was found, indicating no wetting had occurred.

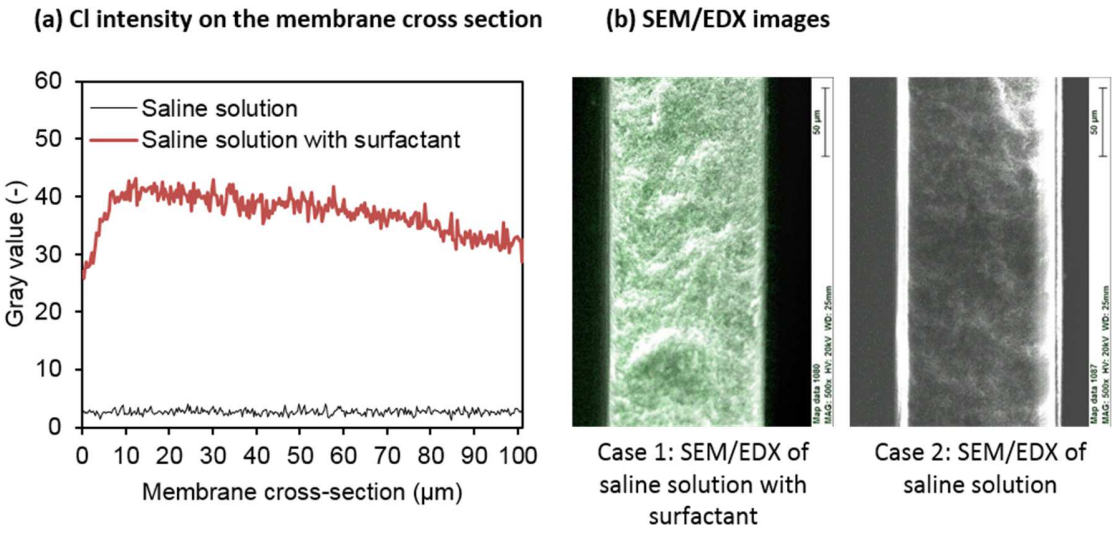


**Figure 8: (a) Chlorine intensity on the membrane cross-section (b) SEM/EDX micrographs for case 1 and case 2 (to be viewed in color)**

These preliminary results allow validating the proof of concept that an increase in light intensity at steady state operation can be linked to a wetting propagation inside the membranes. In the following

section, the membrane was subjected to various feed solutions under steady-state operation, to better illustrate and understand wetting mechanisms.

### 4.2 Influence of surfactant on feed properties, wettability parameters and MD permeate flux

**Table 3** presents the properties of the different solutions used in this study before and after addition of the surfactant in the feed solution where deionized water was used as a control/blank. All measurements were conducted at 25°C and the seawaters were pre-filtered with a 0.45 µm membrane before characterization.

**Table 3: Feed properties and wettability parameters before and after surfactant injection**

| Parameters | Unit | Blank | Without surfactant | | | With surfactant | | |
|---|---|---|---|---|---|---|---|---|
| | | | Saline solution | Seawater 1 | Seawater 2 | Saline solution | Seawater 1 | Seawater 2 |
| Conductivity | mS/cm | 5 x $10^{-5}$ | 51 | 43.8 | 51.1 | 51.5 | 41.1 | 49.5 |
| pH | - | 6.8 | 7 | 7.8 | 7.9 | 7.2 | 7.9 | 8.0 |
| Turbidity | NTU | 0.06 | 0.01 | 0.34 | 0.09 | 0.30 | 0.42 | 1.16 |
| Absorbance UV254nm | - | 0.000 | 0.000 | 0.060 | 0.012 | 0.049 | 0.093 | 0.048 |
| Refractive index | - | 1.33241 | 1.33849 | 1.33754 | 1.33900 | 1.33851 | 1.33719 | 1.33830 |
| Surface tension | mN/m | 72.0 | 73.5 | 73.9 | 72.8 | 62.3 | 64.1 | 57.1 |
| Contact angle | ° | 123.7 | 125.9 | 125.3 | 123.7 | 122.1 | 123.6 | 119.3 |
| LEP | bar | 2.03 | 1.97 | 1.43 | 1.50 | 1.73 | 1.33 | 0.87 |

*Note: All measurements are reported for 25°C*

Considering the different feed properties, an addition of the surfactant generally increased the pH to slightly basic for all samples even though the turbidities of the samples were still clear. Similarly, it could be seen that all samples with an addition of surfactant had an overall increase in refractive index compared to the blank solution. However, after addition of the surfactant, there was a slight reduction in the refractive indexes in the samples. The principal changes in the feed that can be high-lighted is a 15 –

22 % reduction in the surface tension of the feed solution after surfactant addition, implying the wetting potential of the feed solutions had increased.

Concerning the wettability parameters of the feed solutions with the studied membranes, both contact angle and liquid entry pressure were measured. Only a 2-4 % reduction in contact angle was observed, however, LEP presented a 7 to 42 % reduction. It can be seen for LEP that wetting potential of the feed solution after surfactant addition had significantly increased. It worthy to mention that these measurements were taken at standard temperature and pressures. Elevated temperature feed solution with surfactant would have a significant reduction in surface tension thereby increasing the risk of wetting under the operating conditions [29].

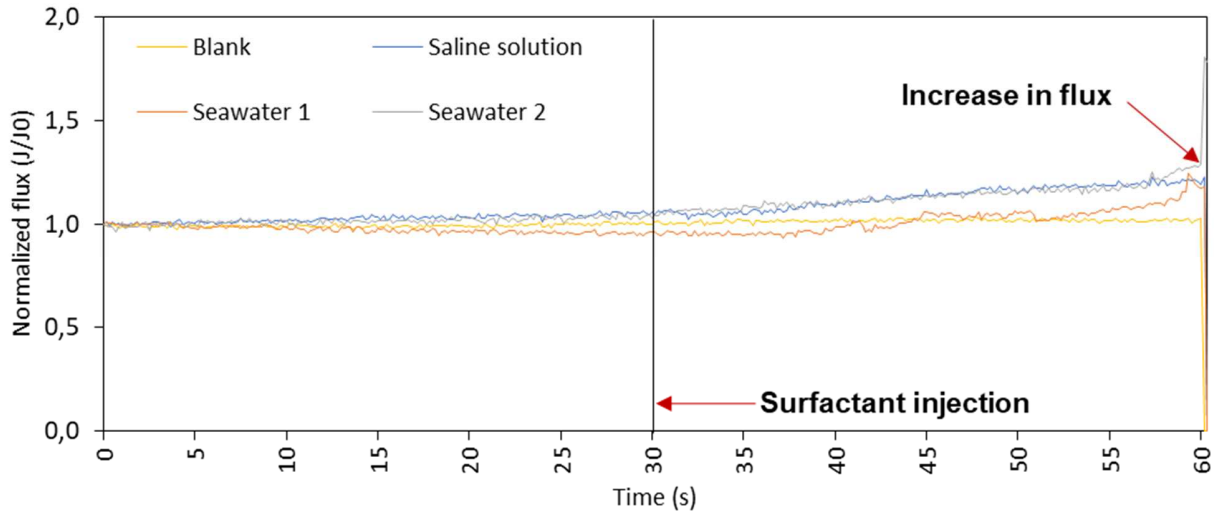


**Figure 9: Flux response for the feed solutions (to be seen in color)**

**Figure** 9 summarizes the normalized flux response in the studied samples under fixed operating conditions. Depending on the samples the permeate flux varied between 2.5 and 3.5 Kg/m².h and generally could be considered stable during the first 30 minutes of operation. However, after addition of the surfactant, a linear trend in flux is observed. This may be attributed to the inward movement of the liquid-vapor interface thereby decreasing the vapor diffusion path and temporarily increasing the flux. Similar observation of an increase in flux leading to wetting, later on, was also observed previously [18]. After 55 min of operation, the vapor flux started to be unstable, and feed solution could be seen to pass

through the membrane in its liquid state confirming total wetting had occurred at some location or locations on the membrane surface during operation.

### 4.3 Visualizing induced wetting with different feed solutions

In this section, the different previously described feed solutions (cf. 3.5) were used to visualize wetting progression under same steady-state operating conditions for 1 hour while using deionized water as blank. Wetting was provoked after 30 min by injecting a surfactant (Triton x) into the feed solution to reach a final concentration of 12.5 ppm.

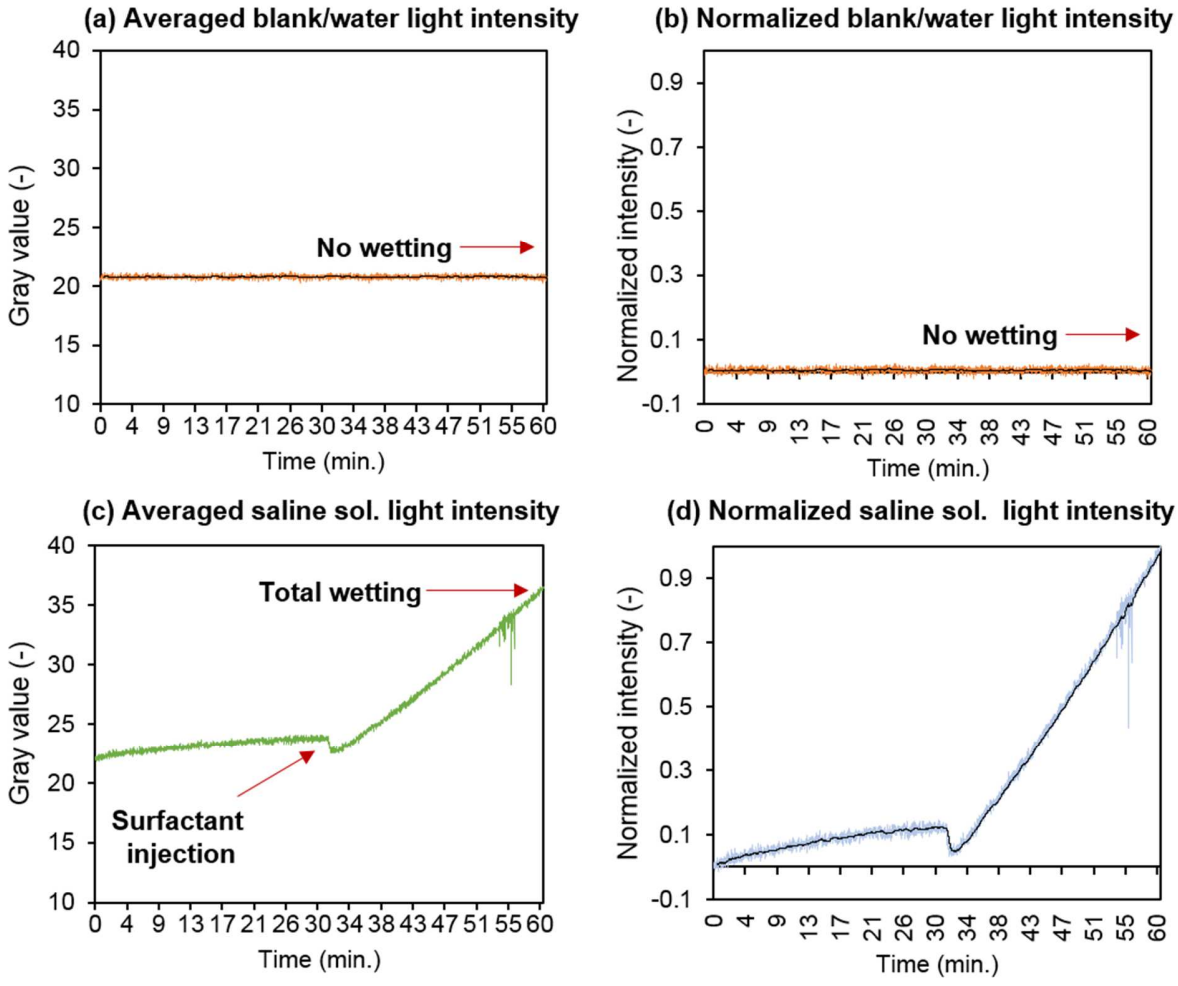

**Figure 10: Averaged and normalized light intensities during experimental run (a, b) blank/water and (c, d) saline solution with surfactant injection after 30 min**

### 4.3.1 Blank and saline solution

**Figure** 10 presents the light transmission with (a) water (blank) and (c) saline solutions for the entire duration of the experiment. In the case of blank, the intensity did not change during the entire operation, and this state could attribute to the steady operating conditions where no wetting occurs. As the feed contained neither salts nor the surfactant; the feed conductivity stayed stable 3.37±0.07 µs/cm. The normalized graph on the right side (**Figure** 10 (b)) also presents the same information. During the total duration of the experiment, no feed liquid had appeared on the permeate side of the membrane surface.

However, considering the saline solution (see **Figure** 10 (c)), the light transmission slightly increased as the experiment continued. This increase in light intensity can be suggested as the inward movement of the L/V interface. However, just after the addition of the surfactant at the ½ hour mark, a sudden drop in light intensity can be observed with a significant increase in light transmission soon afterwards. By the end of the experiment, liquid water appeared on the permeate side of the membrane module validating total wetting had occurred on the membrane surface. Considering the normalized data (**Figure** 10 (d)), surfactant addition into feed solution introduces these molecules at the membrane's liquid vapor interface resulting in a rapid reduction in light intensity. The surfactant interacts with the membrane surface by reducing its hydrophobicity, as well as a reduced membrane contact angle, leading to wetting. Details of progressive nature of surfactant induced wetting can be found elsewhere [29].

### 4.3.2 Seawaters

As the principal application of membrane distillation is for desalination, the application of wetting detection using the optical technique was also tested for real seawaters. Considering light intensities (see **Figure 11**), it can be noted that both samples had lower light transmission than observed for either blank or saline solution. This may be due to additional solutes dissolved in seawater. For the first ½ hour SW1 performed more like the blank with no increase in wetting intensities. However, after the surfactant injection, the intensity dropped like for saline solution but to a lesser extent and then it started to increase. Here the signal was noisy so a running average filter (n=30) was introduced to better visualize the trend in data. The significant noise in the signal was introduced by the surfactant interacting with this

seawater sample and generating small bubbles in the circulating feed samples. As these bubbles passed in front of the visualized membrane surface, they created momentary dark regions resulting in the noisy signal. However, a general trend in the increase in light signal could be still observed.

Considering SW2, this sample had a similar intensity profile as the saline solution. Here it can be noted that there was a slight increase in intensity before the surfactant injection, implying an inward movement in the L/V interface. However, after the surfactant injection, wetting progressed in the same manner as the saline solution. As the surfactant accumulated on the membrane surface there again was a reduction in the intensity and later wetting propagation occurred until a state of total wetting was observed. Total wetting was confirmed by the accumulation of the liquid feed in the permeate side of the membrane.

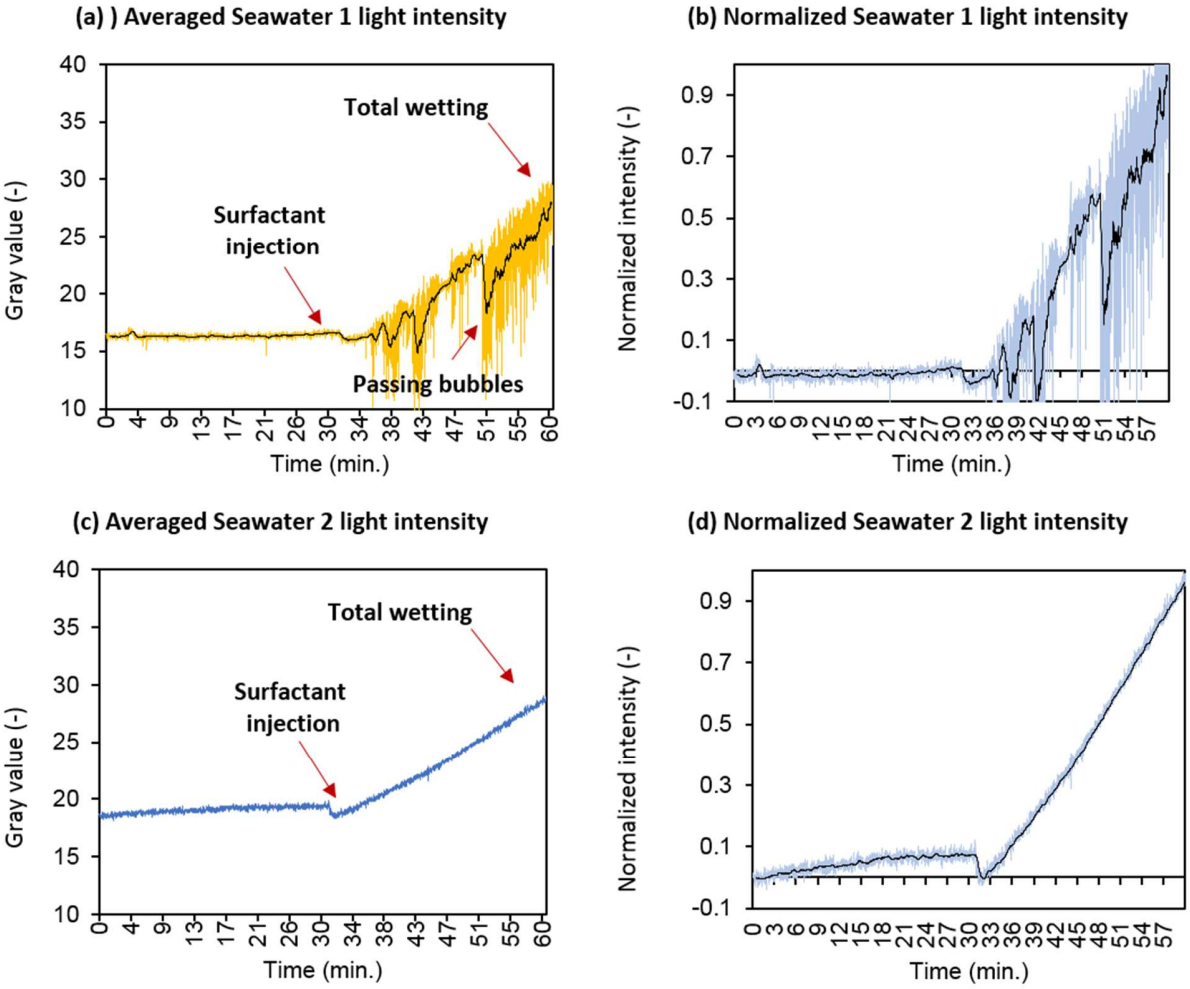

**Figure 11: Averaged and normalized light intensities during experimental run (a and b) seawater 1 (c and d) seawater 2 with surfactant injection after 30 min**

### 4.4 Difference in wetting propagation at macro and meso scale at different locations

Using this optical tool, we can further differentiate wetting occurrences at a more local scale for example at meso scale (0.01 to 30 mm) and compare it with the scale of the membrane. **Figure 12** presents the 4 curves of normalized intensity for the membrane surface at the inlet, middle, outlet and the global intensity for the membrane subjected to the saline solution with the surfactant added at 30 min. The data presented in **Figure 12** is a moving average filter (n=15) to reduce signal noise. Here it can be observed that the global curve match closely to the data sampled at the middle until the surfactant is added. However, wetting propagation at the feed outlet surpasses wetting propagation observed at the inlet and middle of the membrane after surfactant addition. This may be due to the membrane's internal morphology being different at each location or the fluid flow in the membrane feed chamber creating slightly higher localized hydrostatic pressure resulting in faster wetting on the feed outlet. Wetting induction at the feed outlet was faster than that for the inlet and middle even though the overall curves mimic the same linear trend as the global scale. This difference in normalized light intensity is indicative of the change in wetting rate experienced by the same membrane at different locations under the same operating conditions. This level of detail in-situ localized wetting progression was not possible with the current state of the art.

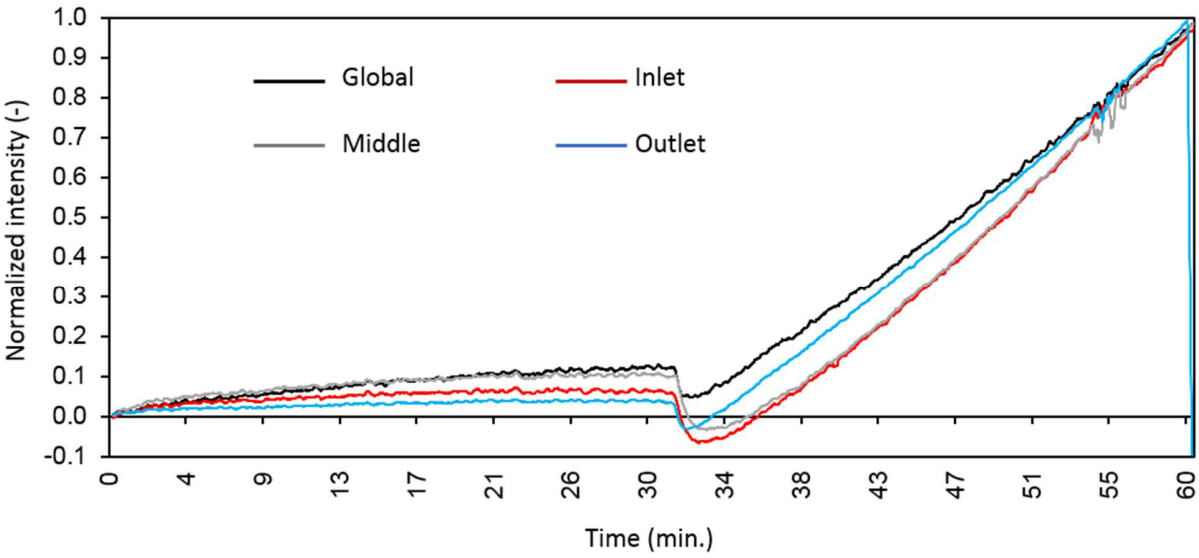

**Figure 12: Comparing wetting progression on the membrane surface at global and local scales: inlet, center and outlet – (To be seen in color)**

Additionally, after the experiment, the membrane was sampled at the inlet location, and $Cl^-$ was profiled by SEM-EDX across the membrane cross-section using pore wetting ratio ($\omega_p$) as presented in **Figure 13** (a and b). Here the progressive change in light intensity can be interpreted by the Cl traces left by the feed solution. The chloride deposits on the feed side membrane cross-section are indicative of an inward movement of the L/V interface leading to surface wetting. The same surface wetting mechanism can also be seen with a slight increase in light intensity from 0- 29 min (see **Figure 13**(c)). However, after surfactant injection, an increase in light intensity could be observed as the liquid vapor interface moved inside the membrane cross-section. At the end of the experiment, the highest intensity (indicated by Normalized data = 1) was observed, indicative of a total wetting and this can be confirmed by the Cl deposits on the permeate side of the membrane cross-section ((see **Figure 13**(b)) Pore wetting ratio also confirms that the total wetted state of the membrane as Cl- peaks can be seen at $\omega_p$ of 97.2 % of the membrane cross-section.

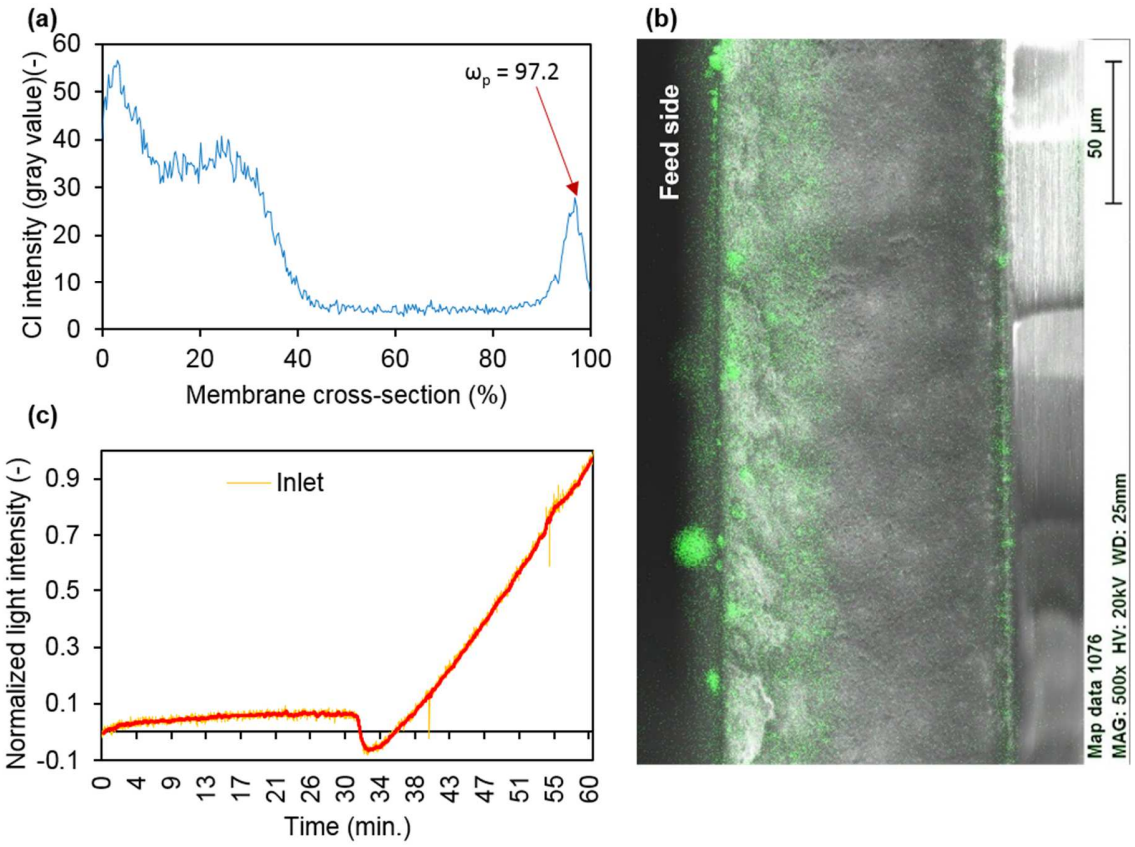


**Figure 13: (a) Chlorine Intensity profile of membrane cross-section (b) SEM/EDX micrograph of the membrane cross-section (c) Normalized in-situ light transmission of at the the same location with saline solution (to be seen in color)**

Wetting progression at the inlet (meso scale) can be validated by the SEM/EDX micrographs at the pore scale. Similar observations can be made all over the membrane surface and used to identify the propagation of wetting mechanisms at different locations. This would enable us to better understand the influence of feed solutions, operating conditions, and process hydrodynamics at a local scale during operation.

The scale and resolution of the wetting observation will depend on the resolution of the camera/sensor setup and area of the membrane visualized. Wetting may not be visualized where the membrane surface is covered for example with the spacer. Wetting propagation may be evaluated on the membrane by precisely determining and correlating SEM/EDX and light at different stages of wetting.

## 5. Conclusions and perspectives

In this study, a non-invasive in-situ optical tool was developed and tested for visualizing wetting propagation in membrane distillation. The proof of concept that in-situ wetting can be detected using light transmission was provided and validated using DDTI method. The tool was tested with saline solutions and seawaters with controlled wetting induced by the surfactant. The optical tool was able to provide information on wetting mechanisms in the studied feed solutions. The developed tool is adaptable and can visualize wetting at both global and local scales. Earlier this level of scalability could be only possible using ex-situ techniques like SEM/EDX.

The developed tool and pore wetting definition is simple and intuitive. The tool can be easily adapted to all membrane distillation configurations for example; DCMD, SGMD, AGMD, and VMD with suitable adaptation the membrane module. With this optical tool, the effects of operating parameters (temperatures, flow rates, local hydrodynamic conditions, feed salinities, time and membrane, etc.) on in-situ wetting can be evaluated. Additional to wetting detection techniques, there is a growing interest in membrane regeneration after wetting. In this study, the proof of concept was based on the observation of de-wetting with the optical method, which also appears as a promising tool to elaborate de-wetting strategies.

The location of the liquid-vapor interface has been proven to be dynamic and dependent on the process operating parameters and membrane material interactions which has shown to be vary significantly. The developed optical tool can visualize and better interpret pore wetting in membrane distillation. **Table 4** summarizes the current advantages of this optical wetting detection tool and further R&D challenges that need to be addressed to make this tool even better.

**Table 4: Advantages and challenges of the developed optical tool**

| Advantages of the optical tool | Challenges to be addressed in future studies |
|---|---|
| • In-situ tool which can evaluate and visualize wetting propagation and mechanisms at the global and local scales | • Wetting visualization is limited by the optics of the camera used therefore wetting can be visualized but not at the scale of the pores (i.e., microscale) |

| Advantages of the optical tool | Challenges to be addressed in future studies |
|---|---|
| • Can be adapted to the main membrane distillation configurations | • Opaque particles / or translucent feed solutions and scaling/fouling may alter visualization of the wetting mechanism |
| • Non-invasive | • Utilization limited to steady state as water properties, and operating parameters may influence light transmission |
| • Non-destructive | • Thin, durable spacers designed to make more of the membrane surface available for visualization, ideally approaching complete surface visualization. |
| • Easy to setup and can be coupled with existing membrane cells with adaptations to visualize the membrane surface | • The optical method needs to be adapted to HF membrane configuration |

1

2

## Acknowledgements

The authors would like to thank ANR (Agence nationale de la recherche) Programme : Innovation technologique pour analyser, remédier ou réduire les risques environnementaux (DS0102) 2014 for funding the projet WETMEM (ANR-14-CE04-0008).

They also acknowledge Manon Montaner, from INSA-TBI for her contribution to the design and manufacturing of the experimental module.

## Nomenclature

| Acronym | Description | Unit |
|---|---|---|
| A | Membrane area | $m^2$ |
| AGMD | Airgap membrane distillation | |
| $a_{oi}$ | Open area of the spacer/opening | $mm^2$ |
| C | Salt concentration | g/L |
| CA | Contact angle | ° |
| D.I. water | De-ionized water | |
| DCMD | Direct contact membrane distillation | |
| DDTI | Detection of Dissolved Tracer Intrusion | |
| E.g. | Example | |
| EDX | Energy-dispersive X-ray spectroscopy | |
| EIC | Electrochemical impedance spectroscopy | |
| F | Flow rate | m/s or L/h |
| FS | Flat sheet | |
| HF | Hollow fiber | |
| i.e. | That is | |
| $I_{avg}$ | Overall average intensity | |
| $I_{initial}$ | Intensity of a reference image where no wetting had occurred | |
| $I_{max}$ | Intensity of an image captured when total wetting had occurred | |
| $I_{observed}$ | Intensity of one image at time (t) | |
| $I_{ROI}$ $(x_i,y_i)$ | Mean light intensity in one ROI | Gray value |
| J | Flux | $Kg/m^2.h$ |
| $K_M$ | Membrane permeability in VMD at 20°C | $s.mol^{1/2}.m^{-1}.kg^{-1/2}$ |
| L/V | Liquid vapor | |
| LED | Light-emitting diode | |

| | | |
|---|---|---|
| $LEP_w$ | Liquid entry pressure with D.I. water | bar |
| MD | Membrane distillation | |
| N | Normalized light intensity | |
| ND | Refractive index | |
| PVDF | Polyvinylidene fluoride | |
| $r_{avg}$ | Average pore radius of the membrane | µm |
| Re | Reynolds number | |
| RGB | Red green blue | |
| RO | Reverse osmosis | |
| ROI | Region of interest | |
| SDS | Sodium dodecyl sulfate | |
| SEM | Scanning electron microscopy | |
| SFE | Surface free energy | mN/m |
| SGMD | Sweeping gas membrane distillation | |
| $S_i$ | Area of one ROI with $x_i$ and $y_i$ as coordinates | |
| ST | Surface tension | mN/m |
| STP | Standard pressure and temperature | |
| T | Temperature | °C or K |
| t | Time | |
| TDS | Total dissolved solids | mg/L |
| $T_f$ | Feed temperature | °C |
| UV | Ultra violet | |
| VMD | Vacuum membrane distillation | |
| w.r.t | With respect to | |
| $x_i$ | Location of one ROI in x direction | |
| $y_i$ | Location of one ROI in y direction | |
| δ | Membrane thickness | µm or m |
| ε | Porosity | |
| ϒ | Surface tension | mN/m |
| $\omega_p$ | Pore wetting ratio | |

## 6. References


[1] E. Drioli, A. Ali, F. Macedonio, Membrane distillation: Recent developments and perspectives, State---Art Rev. Desalination. 356 (2015) 56–84. doi:10.1016/j.desal.2014.10.028.

[2] A. Deshmukh, C. Boo, V. Karanikola, S. Lin, A.P. Straub, T. Tong, D.M. Warsinger, M. Elimelech, Membrane Distillation at the Water-Energy Nexus: Limits, Opportunities, and Challenges, Energy Environ. Sci. (2018).

[3] J.-P. Mericq, S. Laborie, C. Cabassud, Vacuum membrane distillation of seawater reverse osmosis brines, Water Res. 44 (2010) 5260–5273. doi:10.1016/j.watres.2010.06.052.

[4] J.-P. Mericq, S. Laborie, C. Cabassud, Evaluation of systems coupling vacuum membrane distillation and solar energy for seawater desalination, Chem. Eng. J. 166 (2011) 596–606. doi:10.1016/j.cej.2010.11.030.

[5] A. Kujawska, J.K. Kujawski, M. Bryjak, M. Cichosz, W. Kujawski, Removal of volatile organic compounds from aqueous solutions applying thermally driven membrane processes. 2. Air gap membrane distillation, J. Membr. Sci. 499 (2016) 245–256. doi:10.1016/j.memsci.2015.10.047.

[6] E. Guillen-Burrieza, M.O. Mavukkandy, M.R. Bilad, H.A. Arafat, Understanding wetting phenomena in membrane distillation and how operational parameters can affect it, J. Membr. Sci. 515 (2016) 163–174. doi:10.1016/j.memsci.2016.05.051.

[7] P. Jacob, S. Laborie, C. Cabassud, Visualizing and evaluating wetting in membrane distillation: New methodology and indicators based on Detection of Dissolved Tracer Intrusion (DDTI), Desalination. 443 (2018) 307–322. doi:10.1016/j.desal.2018.06.006.

[8] K. Smolders, A.C.M. Franken, Terminology for Membrane Distillation, Desalination. 72 (1989) 249–262. doi:10.1016/0011-9164(89)80010-4.

[9] M. Gryta, Influence of polypropylene membrane surface porosity on the performance of membrane distillation process, J. Membr. Sci. 287 (2007) 67–78.

[10] S.A. Hashemifard, T. Matsuura, A.F. Ismail, M. Rezaei Dasht Arzhandi, D. Rana, G. Bakeri, Characterization of partial pore wetting in hollow fiber gas absorption membrane contactors: An EDX analysis approach, Chem. Eng. J. 281 (2015) 970–980. doi:10.1016/j.cej.2015.07.036.

[11] F.E. Ahmed, B.S. Lalia, R. Hashaikeh, Membrane-based detection of wetting phenomenon in direct contact membrane distillation, J. Membr. Sci. (2017). doi:10.1016/j.memsci.2017.04.035.

[12] Y. Chen, Z. Wang, G.K. Jennings, S. Lin, Probing Pore Wetting in Membrane Distillation Using Impedance: Early Detection and Mechanism of Surfactant-Induced Wetting, Environ. Sci. Technol. Lett. (2017). doi:10.1021/acs.estlett.7b00372.

[13] P. Jacob, T. Zhang, S. Laborie, C. Cabassud, Influence of operating conditions on wetting and wettability in membrane distillation using Detection of Dissolved Tracer Intrusion (DDTI), Desalination. 468 (2019) 114086. doi:10.1016/j.desal.2019.114086.

[14] E. Guillen-Burrieza, R. Thomas, B. Mansoor, D. Johnson, N. Hilal, H. Arafat, Effect of dry-out on the fouling of PVDF and PTFE membranes under conditions simulating intermittent seawater membrane distillation (SWMD), J. Membr. Sci. 438 (2013) 126–139.

[15] M. Gryta, The study of performance of polyethylene chlorinetrifluoroethylene membranes used for brine desalination by membrane distillation, Desalination. 398 (2016) 52–63. doi:10.1016/j.desal.2016.07.021.

[16] M. Gryta, J. Grzechulska-Damszel, A. Markowska, K. Karakulski, The influence of polypropylene degradation on the membrane wettability during membrane distillation, J. Membr. Sci. 326 (2009) 493–502. doi:10.1016/j.memsci.2008.10.022.

[17] V. Chen, H. Li, A.G. Fane, Non-invasive observation of synthetic membrane processes – a review of methods, J. Membr. Sci. 241 (2004) 23–44. doi:10.1016/j.memsci.2004.04.029.

[18] M. Gryta, Long-term performance of membrane distillation process, J. Membr. Sci. 265 (2005) 153–159.

[19] M. Gryta, M. Barancewicz, Influence of morphology of PVDF capillary membranes on the performance of direct contact membrane distillation, J. Membr. Sci. 358 (2010) 158–167. doi:10.1016/j.memsci.2010.04.044.

[20] K.W. Lawson, D.R. Lloyd, Membrane distillation. I. Module design and performance evaluation using vacuum membrane distillation, J. Membr. Sci. 120 (1996) 111–121.

[21] L. Peña, J.M.O. de Zárate, J.I. Mengual, Steady states in membrane distillation: Influence of membrane wetting, J. Chem. Soc. Faraday Trans. 89 (1993) 4333–4338.

[22] L.D. Nghiem, F. Hildinger, F.I. Hai, T. Cath, Treatment of saline aqueous solutions using direct contact membrane distillation, Desalination Water Treat. 32 (2011) 234–241.

[23] E. Guillen-Burrieza, A. Ruiz-Aguirre, G. Zaragoza, H.A. Arafat, Membrane fouling and cleaning in long term plant-scale membrane distillation operations, J. Membr. Sci. 468 (2014) 360–372.

[24] R.B. Saffarini, B. Mansoor, R. Thomas, H.A. Arafat, Effect of temperature-dependent microstructure evolution on pore wetting in PTFE membranes under membrane distillation conditions, J. Membr. Sci. 429 (2013) 282–294. doi:10.1016/j.memsci.2012.11.049.

[25] J. Hou, M.Y. Zulkifli, M. Mohammad, Y. Zhang, A. Razmjou, V. Chen, Biocatalytic gas-liquid membrane contactors for CO 2 hydration with immobilized carbonic anhydrase, J. Membr. Sci. 520 (2016) 303–313.

[26] A. McLeod, B. Jefferson, E.J. McAdam, Toward gas-phase controlled mass transfer in micro-porous membrane contactors for recovery and concentration of dissolved methane in the gas phase, J. Membr. Sci. 510 (2016) 466–471.

[27] S.-H. Yeon, K.-S. Lee, B. Sea, Y.-I. Park, K.-H. Lee, Application of pilot-scale membrane contactor hybrid system for removal of carbon dioxide from flue gas, J. Membr. Sci. 257 (2005) 156–160.

[28] C. Duan, W.-N. Mei, W.-G. Yin, J. Liu, J. Hardy, M. Bai, S. Ducharme, Theoretical study on the optical properties of polyvinylidene fluoride crystal, J. Phys. Condens. Matter. 15 (2003) 3805.

[29] Z. Wang, Y. Chen, X. Sun, R. Duddu, S. Lin, Mechanism of pore wetting in membrane distillation with alcohol vs. surfactant, J. Membr. Sci. 559 (2018) 183–195. doi:10.1016/j.memsci.2018.04.045.

[30] L. Han, Y.Z. Tan, T. Netke, A.G. Fane, J.W. Chew, Understanding oily wastewater treatment via membrane distillation, J. Membr. Sci. 539 (2017) 284–294. doi:10.1016/j.memsci.2017.06.012.

[31] T.D. Dao, J.-P. Mericq, S. Laborie, C. Cabassud, A new method for permeability measurement of hydrophobic membranes in Vacuum Membrane Distillation process, Water Res. 47 (2013) 2096–2104. doi:10.1016/j.watres.2013.01.040.

[32] Y.Z. Tan, L. Han, W.H. Chow, A.G. Fane, J.W. Chew, Influence of module orientation and geometry in the membrane distillation of oily seawater, Desalination. 423 (2017) 111–123. doi:10.1016/j.desal.2017.09.019.

[33] A. Siddiqui, N. Farhat, S.S. Bucs, R.V. Linares, C. Picioreanu, J.C. Kruithof, M.C. van Loosdrecht, J. Kidwell, J.S. Vrouwenvelder, Development and characterization of 3D-printed feed spacers for spiral wound membrane systems, Water Res. 91 (2016) 55–67.

[34] N. Sreedhar, N. Thomas, O. Al-Ketan, R. Rowshan, H. Hernandez, R.K. Abu Al-Rub, H.A. Arafat, 3D printed feed spacers based on triply periodic minimal surfaces for flux enhancement and biofouling mitigation in RO and UF, Desalination. 425 (2018) 12–21. doi:10.1016/j.desal.2017.10.010.

[35] N. Thomas, N. Sreedhar, O. Al-Ketan, R. Rowshan, R.K. Abu Al-Rub, H. Arafat, 3D printed triply periodic minimal surfaces as spacers for enhanced heat and mass transfer in membrane distillation, Desalination. 443 (2018) 256–271. doi:10.1016/j.desal.2018.06.009.

[36] M. Monnot, H.T.K. Nguyên, S. Laborie, C. Cabassud, Seawater reverse osmosis desalination plant at community-scale: Role of an innovative pretreatment on process performances and intensification, EPIC2015. 113 (2017) 42–55. doi:10.1016/j.cep.2016.09.020.

[37] J. Schindelin, I. Arganda-Carreras, E. Frise, V. Kaynig, M. Longair, T. Pietzsch, S. Preibisch, C. Rueden, S. Saalfeld, B. Schmid, Fiji: an open-source platform for biological-image analysis, Nat. Methods. 9 (2012) 676.